

Energy-Efficient Multi-UAV-Enabled MEC Systems with Space-Air-Ground Integrated Networks

Wenchao Liu, *Student Member, IEEE*, Xuhui Zhang, *Student Member, IEEE*, Jinke Ren, *Member, IEEE*, Yanyan Shen, *Member, IEEE*, Shuqiang Wang, *Senior Member, IEEE*, Bo Yang, *Senior Member, IEEE*, Xinping Guan, *Fellow, IEEE*, and Shuguang Cui, *Fellow, IEEE*

Abstract—With the development of artificial intelligence integrated next-generation communication networks, mobile users (MUs) are increasingly demanding the efficient processing of computation-intensive and latency-sensitive tasks. However, existing mobile computing networks struggle to support the rapidly growing computational needs of the MUs. Fortunately, space-air-ground integrated network (SAGIN) supported mobile edge computing (MEC) is regarded as an effective solution, offering the MUs multi-tier and efficient computing services. In this paper, we consider an SAGIN supported MEC system, where a low Earth orbit satellite and multiple unmanned aerial vehicles (UAVs) are dispatched to provide computing services for MUs. An energy efficiency maximization problem is formulated, with the joint optimization of the MU-UAV association, the UAV trajectory, the task offloading decision, the computing frequency, and the transmission power control. Since the problem is non-convex, we decompose it into four subproblems, and propose an alternating optimization based algorithm to solve it. Simulation results confirm that the proposed algorithm outperforms the benchmarks.

Index Terms—Space-air-ground integrated network (SAGIN), multiple unmanned aerial vehicles (UAVs), energy-efficient mobile edge computing (MEC), resource allocation, trajectory design.

I. INTRODUCTION

THE advancements in mobile communication networks have led to an exponential increase in the demand for ubiquitous access from mobile users (MUs) [1]. Despite the significant enhancement of terrestrial network convenience afforded by the fifth-generation (5G) technology, connectivity

issues, such as weak wireless access capability and unsatisfied computing services, still exist in areas with sparse MUs, due to the limitations in coverage and economic costs [2]. To address these issues and achieve pervasive connectivity in remote regions, the integration of non-terrestrial networks has emerged as a promising strategy in the next-generation communication systems [3] to provide ubiquitous services for the MUs.

Space-air-ground integrated network (SAGIN), as a typical non-terrestrial network, includes three primary components: the space-based network, which includes low Earth orbit (LEO) satellites; the air-based network, encompassing aircraft, unmanned aerial vehicles (UAVs), and high-altitude platforms; and the ground-based network, consisting of terrestrial base stations, MUs, and Internet of Things (IoT) devices [4]. Satellite-enabled non-terrestrial networks can provide the MUs with extensive connectivity across both territory and time [5]. However, due to the long distance between the satellites and the ground, it faces challenges such as high transmission latency, low transmission rates, and increased energy consumption for long-distance transmissions. In contrast, terrestrial communication performs excellently in urban areas with the high density of MUs, providing high-speed and low-latency services [6]. However, due to its limited coverage, it struggles to meet the communication needs of MUs located in remote regions [7]. To tackle this issue, the UAVs can serve as aerial communication devices to provide communication and computing services. Due to their agile mobility, the UAVs can offer more flexible coverage and more stable communication quality for the MUs [8]. Through this multi-tier connectivity of the SAGIN, the MUs can benefit from the diverse services offered by different service providers including the LEO satellites and the UAVs, thereby the quality of services of all MUs can be improved [9], [10].

Furthermore, the widespread utilization of those famous computation-intensive and latency-sensitive tasks and devices, including the multimedia applications, social networks, and emerging intelligent devices such as wearable devices and smart home controllers, has significantly impacted the MUs. The increase in usage has heightened the demand for efficient communication connectivity and high-speed data transmission. Additionally, it has highlighted the importance of enhancing the processing capabilities of the MUs to effectively manage the growing task loads. As a result, optimizing task processing performance has become a critical issue deserving urgent attention [11], [12]. This requires efficient and reliable commu-

W. Liu is with Shenzhen Institute of Advanced Technology, Chinese Academy of Sciences, Guangdong 518055, China, and also with Southern University of Science and Technology, Guangdong 518055, China (e-mail: wc.liu1@siat.ac.cn).

X. Zhang and J. Ren are with the Shenzhen Future Network of Intelligence Institute, the School of Science and Engineering, and the Guangdong Provincial Key Laboratory of Future Networks of Intelligence, The Chinese University of Hong Kong, Shenzhen, Guangdong 518172, China (e-mail: xu.hui.zhang@foxmail.com; jinkeren@cuhk.edu.cn).

Y. Shen and S. Wang are with the Shenzhen Institute of Advanced Technology, Chinese Academy of Sciences, Guangdong 518055, China, and also with Shenzhen University of Advanced Technology, Guangdong 518055, China (e-mail: yy.shen@siat.ac.cn; sq.wang@siat.ac.cn).

B. Yang and X. Guan are with the Department of Automation and the Key Laboratory of System Control and Information Processing, Ministry of Education, Shanghai Jiao Tong University, Shanghai 200240, China (e-mail: bo.yang@sjtu.edu.cn; xpguan@sjtu.edu.cn).

S. Cui is with the School of Science and Engineering, the Shenzhen Future Network of Intelligence Institute, and the Guangdong Provincial Key Laboratory of Future Networks of Intelligence, The Chinese University of Hong Kong, Shenzhen, Guangdong 518172, China (e-mail: shuguangcui@cuhk.edu.cn).

nication and computing resources. However, traditional cloud-centric computing models struggle to provide the MUs located at remote areas with high-quality user experiences. To address this issue, mobile edge computing (MEC) has been proposed as a solution that efficiently utilizes computational resources at the network edge [13]. The MEC brings computing and storage resources to the edge of the mobile network, placing them closer to the ground MUs. Through localized data processing and real-time analysis, the energy consumption and latency of task processing can be reduced, and the adaptability of the network is also enhanced [14].

However, effectively utilizing computing resources in the SAGIN supported MEC systems to enhance task processing efficiency remains a topic requiring further investigation to address various challenges. Firstly, the maximum processing latency of tasks must be considered to ensure that the data processing time satisfies the latency requirements. Secondly, the MUs and the aerial computing platforms such as the UAVs and high-altitude platforms often have limited energy capacity, necessitating the optimized energy usage to extend their battery lifetimes. Additionally, the dynamic nature of the network increase the complexity of resource allocation and task scheduling, requiring efficient algorithms to address these challenges.

To the best of our knowledge, there is a lack of study on the multi-level computation offloading in SAGIN that considers the MU-UAV association and resource allocation for multiple UAVs with their controllable flying trajectories, while meeting the latency requirements of the MUs. To fill this research gap, this article investigates an SAGIN-supported MEC system that jointly considers the MU-UAV association, the multiple UAVs trajectory design, transmit power allocation, task offloading decisions, and computing frequency allocation. The main contributions can be summarized as follows:

- Firstly, we propose a novel SAGIN-supported MEC system with multiple UAVs, aiming at achieving extensive coverage and hotspot communication enhancement. Under the constraints of maximum latency of the MU tasks and maximum energy consumption of the UAVs, we aim to maximize the total energy efficiency of the system through jointly optimizing the MU-UAV association, the UAV trajectory, task offloading decision, transmit power control and computing frequency control.
- Secondly, due to the coupling between variables, the binary nature of the MU-UAV association, and the fractional structure in the objective function, the initial problem becomes a non-convex mixed-integer non-linear optimization problem. We first utilize quadratic transformation to eliminate the fractional structure, then apply an alternating optimization (AO)-based algorithm to decompose and solve the problem.
- Numerical results illustrate the impact of different parameters in the considered SAGIN-supported MEC system, such as the number of MUs, the data size of tasks required for processing, and the bandwidth among the MUs and the UAVs, on the achievable performance. The results also highlight the benefits of optimizing the UAV trajectories, optimizing the offloading allocations, and

adjusting the number of UAVs. Additionally, the results display the UAV trajectories and the changes in task allocation over time.

The remainder of this article is organized as follows. In Section II, we discuss the existing related works in details. Section III introduces the system model, and provides the problem formulation. In Section IV, we introduce the proposed AO-based algorithm and offers convergence and complexity analysis. Section V evaluates the performance of the proposed algorithm through numerical analysis. Finally, in Section VI, we summarize this article.

II. RELATED WORKS

Currently, some pioneering works began to explore the deployment of SAGIN in next-generation communication networks [15]–[23]. Benefited from the global coverage capabilities of the LEO satellites, the SAGIN can provide a new approach for achieving seamless coverage and enhancing the ubiquitous computing services. Specifically, Chen et al. [15] proposed an intelligent user association strategy in a novel SAGIN system, and the capacity and coverage probability are also analysed. Wang et al. [16] exploited the target positioning in a maritime SAGIN system, where the direction-of-arrival of the targets were estimated by the UAVs. Mohamed et al. [17] studied the joint UAV trajectory planning and LEO satellite selection, and the user data rate was maximized. Tang et al. [18] proposed a learning based network traffic control for SAGIN by considering the high mobility of users as well as frequent changing network traffic and link state. Besides, the joint deployment and optimization of the SAGIN and next-generation communication technologies, including the backscatter communications [19], the blockchain-enabled systems [20], [21], the IoT data collections [22], and the reconfigurable intelligent surface-assisted systems [23], have been studied. However, the increasing demand for the computing tasks by the emerging applications from the MUs still cannot be satisfied.

Fortunately, the MEC system, as a new distributed computing paradigm based on wireless communication networks, has attracted widespread attentions. Several pioneer works [24]–[31] started to investigate the computing potential of the implementation of the MEC systems towards next-generation wireless communication networks. Ren et al. investigated the resource allocation [24], and the collaboration of cloud computing and edge computing [25] to minimize the latency of all mobile devices. Cao et al. [26] proposed a new cooperation method in both computation and communication resources for MEC systems to improve the energy efficiency. Wang et al. [27] studied a wireless powered MEC system, where the total transmission energy consumption was minimized considering both energy and task causality constraints. Zhang et al. [28] optimized the sum of utilities, which jointly considered the energy efficiency, time latency, and price of offloading computations in an intelligent reflecting surface aided MEC system. Liang et al. [29] studied the joint task offloading, communication, and computation resource allocation in a multi-user MEC system. Meanwhile, the UAV-enabled MEC

systems were studied in [30], [31], where the systems are benefited by the mobility of the UAV through optimizing the UAV trajectories and resource allocations. Nevertheless, these works mainly focused on the terrestrial networks. The MUs in remote areas are still unable to utilize cloud and edge computing resources to handle computational tasks due to the lack of effective network access.

Introducing the SAGIN into the MEC systems has become a key emerging approach to address the aforementioned issues. Notably, the LEO satellites provide extensive global coverage, while the UAVs offer flexible deployment and dynamic response capabilities. This combination not only compensates for the limitations of single networks but also delivers more stable and efficient computing and communication services across various application scenarios, significantly enhancing task processing efficiency. There has been several works dedicated to developing strategies for efficient task processing and computing resource management in SAGIN-supported MEC systems [32]–[35]. Specifically, Huang et al. [32] studied the minimization of total energy consumption for task processing in a SAGIN-supported MEC system. Hu et al. [33] focused on the maximization of total energy efficiency by jointly optimizing the trajectories of two UAVs with different operations, computing resource allocation, and bandwidth allocation. Nguyen et al. [34] studied the computation offloading problem in hybrid edge-cloud based SAGIN, where the total system energy consumption was minimized. Du et al. [35] presented an MEC and blockchain enabled SAGIN architecture, while minimized the energy consumption through the task segmentation, the UAVs and satellite's bandwidth allocation among their served IoT devices. Nonetheless, to enhance the quality of service for the MUs, the multiple UAV control and the association of the UAV to their served MUs remain pressing issues that need to be addressed. These challenges are often overlooked in existing works.

III. SYSTEM MODEL AND PROBLEM FORMULATION

As depicted in Fig. 1, we consider an SAGIN-supported MEC system, which consists of M MUs, denoted as $\mathcal{M} = \{1, 2, \dots, M\}$, K UAVs, denoted as $\mathcal{K} = \{1, 2, \dots, K\}$, and an LEO satellite. The LEO satellite and each UAV are equipped with an onboard computing server, which can provide computing services to the MUs. Meanwhile, each MU has a computation task, which can be separated into several independent and fine-grained subtasks [36]. Due to the computing latency requirements of the tasks and the limited computational capabilities of the MUs, a portion of these tasks need to be offloaded to the UAVs and the LEO satellite for remote computing.

We consider a time period \mathcal{T} with N time slots, denoted as $\mathcal{N} = \{1, 2, \dots, N\}$, with each time slot having equal duration τ . At the beginning of each time slot, a task will be generated at each MU. The hybrid time division and frequency division multiple access is considered [37]. Since the duration τ is very small, the position of the UAV during each time slot is fixed, while varies across different time slots. It is assumed that the UAVs fly at a fixed altitude H , which enables them

to fly smoothly and avoid obstacles and buildings. Hence, the position of the UAV k can be denoted as $\mathcal{Q}_k[n] = (\mathbf{q}_k[n], H)$, where $\mathbf{q}_k[n] = (x_k[n], y_k[n])$ is the horizontal coordinates. Moreover, the location of the MU m is denoted as $\mathcal{S}_m[n] = (s_m[n], 0)$, where $s_m[n] = (x_m[n], y_m[n])$.

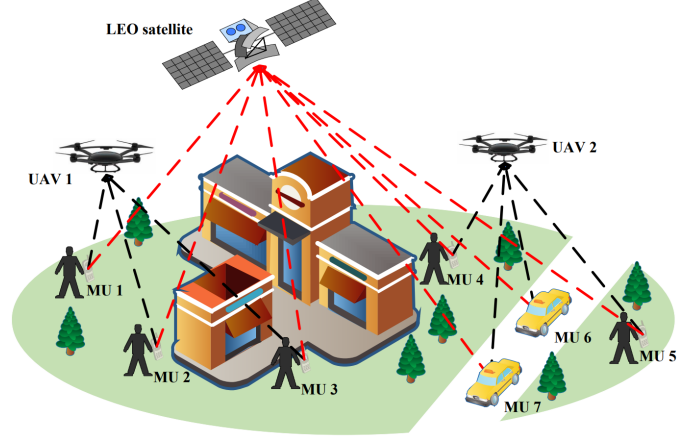


Fig. 1: System model of the space-air-ground integrated MEC.

A. UAV Kinetic Model

The initial and final positions of each UAV are defined as $\mathbf{q}_k[1] = \mathbf{q}_{k,1}$, $\mathbf{q}_k[N] = \mathbf{q}_{k,F}$, $\forall k$, respectively. To ensure the flight stability of all UAVs, the constraint that avoids the collisions among the UAVs, and the constraint for the UAV speed must be satisfied, which are given by

$$\begin{aligned} d_{\min}^2 &\leq \|\mathbf{q}_k[n] - \mathbf{q}_i[n]\|^2, \quad \forall k, i \in \mathcal{K}, i \neq k, \forall n \in \mathcal{N}, \quad (1) \\ \|\mathbf{v}_k[n]\| &= \frac{\|\mathbf{q}_k[n] - \mathbf{q}_k[n-1]\|}{\tau} \leq V_{\max}, \quad \forall k, \forall n \in \mathcal{N} \setminus \{1\}, \quad (2) \end{aligned}$$

where d_{\min} denotes the minimum safe distance between any two UAVs, and V_{\max} denotes the maximum speed of the UAVs. Furthermore, the energy consumption for the flight of the UAV k can be expressed as

$$E_k^{\text{prop}}[n] = \tau \left(\zeta_1 \|\mathbf{v}_k[n]\|^3 + \frac{\zeta_2}{\|\mathbf{v}_k[n]\|} \right), \quad (3)$$

where ζ_1 and ζ_2 are fixed parameters related to the UAV's weight, wing area, air density, etc [38].

B. Communication Model

We assume that each MU is equipped with two communication interfaces: one for communicating with the LEO satellite and another for communicating with the associated UAV. The two interfaces operate on distinct spectral bands, ensuring that there is no interference between the communications with the UAVs and the communications with the LEO satellite [39], [40].

Due to the flexibility of the UAVs, they can fly close to MUs to establish line-of-sight (LoS) links. The channel gain between the MU m and UAV k can be expressed as

$$h_{m,k}[n] = \frac{\beta_0}{d_{m,k}^2[n]} = \frac{\beta_0}{H^2 + \|\mathbf{q}_k[n] - \mathbf{s}_m[n]\|^2}, \quad (4)$$

where β_0 represents the channel gain at the reference distance $d_0 = 1\text{m}$. Thus, the transmission rate from MU m to UAV k can be expressed as

$$R_{m,k}[n] = B_{m,k} \log_2 \left(1 + \frac{p_{m,k}[n]h_{m,k}[n]}{\sigma_{\text{UAV}}^2} \right), \quad (5)$$

where $B_{m,k}$ denotes the bandwidth allocated for data transmission between MU m and UAV k , $p_{m,k}[n]$ is the transmit power of MU m for communicating with UAV k , and σ_{UAV}^2 is the noise power.

Besides, a portion of the task of MUs can be offloaded to the LEO satellite for computing. Accordingly, the channel conditions between the MUs and the LEO satellite are primarily influenced by the distance and meteorological environment. We assume that the meteorological environment remains constant during the task processing period, hence the channel gain between each MU and the LEO satellite is predominantly determined by the satellite's altitude [11], [40], [41]. Thus, the transmission rate between the MU m and the LEO satellite can be expressed as

$$R_{m,\text{LEO}}[n] = B_{\text{LEO}} \log_2 \left(1 + \frac{p_{m,\text{LEO}}[n]|g_{m,\text{LEO}}|^2}{\sigma_{\text{LEO}}^2} \right), \quad (6)$$

where B_{LEO} denotes the bandwidth allocated for data transmission between each MU and the LEO satellite, $p_{m,\text{LEO}}$ denotes the transmit power of the MU m for communicating with the LEO satellite, $g_{m,\text{LEO}}$ is the channel gain between the MU m and the LEO satellite, and σ_{LEO}^2 is the noise power.

C. Computing Model

At the beginning of each time slot, each MU arrives a task, denoted as $\{D_m[n], \phi_m[n]\}$, where $D_m[n]$ represents the data size of the task, and $\phi_m[n]$ represents the computing cycles required to process one bit data. Let $\{\omega_m^L[n], \omega_m^U[n], \omega_m^S[n]\}$ denote the set of task offloading decision of the MU m , where $\omega_m^L[n], \omega_m^U[n], \omega_m^S[n] \in [0, 1]$ represent the proportions of tasks processed locally, offloaded to the associated UAV, and offloaded to the LEO satellite, respectively. The task offloading decision satisfies $\omega_m^L[n] + \omega_m^U[n] + \omega_m^S[n] = 1, \forall m, n$.

a) *Local Processing*: Let $f_m^L[n]$ denote the number of computing cycles per second of the MU m at time slot n . Then, the latency for processing $\omega_m^L[n]D_m[n]$ -bit task locally at the MU m is

$$L_m^L[n] = \frac{\omega_m^L[n]D_m[n]\phi_m[n]}{f_m^L[n]}. \quad (7)$$

Accordingly, the energy consumption for local processing is

$$E_m^L[n] = \kappa_L (f_m^L[n])^2 \omega_m^L[n] D_m[n] \phi_m[n], \quad (8)$$

where κ_L denotes the energy efficiency factor for the local computing of all MUs.

b) *UAV Processing*: When the MU m offloads a partial task $\omega_m^U[n]D_m[n]$ to the associated UAV, the latency comprises three parts: the time for task data uplink transmission from the MU to the associated UAV, the time for the task computation at the associated UAV, and the time for task computation result downlink transmission from the UAV to the MU. Since the

data volume of the results is much smaller than that of the offloaded task, the download latency can be neglected [11].

Each MU is associated with a specified UAV per time slot, and a portion of their tasks can be offloaded to the associated UAV for computing. We introduce a binary indicator $\alpha_{m,k}[n]$ to denote the association, where $\alpha_{m,k}[n] = 1$ indicates that the MU m is associated with the UAV k at time slot n , otherwise $\alpha_{m,k}[n] = 0$. Let $f_{m,k}^U[n]$ denote the number of computing cycles per second that UAV k allocates to MU m . The latency for completing the $\omega_m^U[n]D_m[n]$ -bit task at the UAV k consists of two parts: the task offloading and the task processing. Therefore, the latency can be expressed as

$$L_m^U[n] = \sum_{k=1}^K \alpha_{m,k}[n] \left(\frac{\omega_m^U[n]D_m[n]}{R_{m,k}[n]} + \frac{\omega_m^U[n]D_m[n]\phi_m[n]}{f_{m,k}^U[n]} \right). \quad (9)$$

Hence, the energy consumption of MU m for offloading task to the associated UAV and the energy consumption for processing the task by UAV k are given respectively by

$$E_m^{\text{U,tran}}[n] = \sum_{k=1}^K \alpha_{m,k}[n] \frac{p_{m,k}[n]\omega_m^U[n]D_m[n]}{R_{m,k}[n]}, \quad (10)$$

$$E_{m,k}^{\text{U,com}}[n] = \alpha_{m,k}[n]\kappa_U (f_{m,k}^U[n])^2 \omega_m^U[n] D_m[n] \phi_m[n], \quad (11)$$

where κ_U denotes the energy efficiency factor for task processing of the UAVs.

c) *LEO Satellite Processing*: Similar to the tasks processed by the UAVs, the latency of the tasks processed by the LEO satellite also consists of two parts: the latency for offloading tasks from the MU to the LEO satellite and the latency for task computation at the LEO satellite. Let $f_m^S[n]$ denote the number of computing cycles per second that the LEO satellite allocates to MU m . The latency for processing $\omega_m^S[n]D_m[n]$ -bit task from MU m at the LEO satellite can be expressed as

$$L_m^S[n] = \frac{\omega_m^S[n]D_m[n]}{R_{m,\text{LEO}}[n]} + \frac{\omega_m^S[n]D_m[n]\phi_m[n]}{f_m^S[n]}. \quad (12)$$

Accordingly, the energy consumption for task offloading from MU m to the LEO satellite and the energy consumption for processing the task are given by

$$E_m^{\text{S,tran}}[n] = \frac{p_{m,\text{LEO}}[n]\omega_m^S[n]D_m[n]}{R_{m,\text{LEO}}[n]}, \quad (13)$$

$$E_m^{\text{S,com}}[n] = \kappa_S (f_m^S[n])^2 \omega_m^S[n] D_m[n] \phi_m[n], \quad (14)$$

where κ_S denotes the energy efficiency factor for task computing of the LEO satellite.

To this end, the total latency and total energy consumption of MU m are given by

$$L_m^{\text{sum}}[n] = \max \{ L_m^L[n], L_m^U[n], L_m^S[n] \}, \quad (15)$$

$$E_m^{\text{sum}}[n] = E_m^L[n] + E_m^{\text{U,tran}}[n] + \sum_{k \in \mathcal{K}} E_{m,k}^{\text{U,com}}[n] + E_m^{\text{S,tran}}[n] + E_m^{\text{S,com}}[n]. \quad (16)$$

D. Problem Formulation

In this work, we aim to maximize the total energy efficiency of the system by jointly optimizing the UAV trajectory $\mathbf{Q} = \{\mathbf{q}_k[n], \forall k, n\}$, the transmit power of all MUs $\mathbf{P} = \{p_{m,k}[n], p_{m,\text{LEO}}[n], \forall m, k, n\}$, the task offloading decision of all MUs $\mathbf{\Omega} = \{\omega_m^L[n], \omega_m^U[n], \omega_m^S[n], \forall m, n\}$, the association among the MUs and the UAVs $\mathbf{\alpha} = \{\alpha_{m,k}[n], \forall m, k, n\}$, and the computing frequency allocation of the MUs, the UAVs and the LEO satellite $\mathbf{F} = \{f_m^L[n], f_{m,k}^U[n], f_m^S[n], \forall m, k, n\}$. The problem can be formulated as

$$\mathbf{P1:} \quad \max_{\{\mathbf{Q}, \mathbf{P}, \mathbf{\Omega}, \mathbf{F}, \mathbf{\alpha}\}} \sum_{m=1}^M \sum_{n=1}^N \frac{D_m[n]}{E_m^{\text{sum}}[n]} \quad (17a)$$

$$\text{s.t. } \mathbf{q}_k[1] = \mathbf{q}_{k,1}, \mathbf{q}_k[N] = \mathbf{q}_{k,N}, \forall k, \quad (17b)$$

$$d_{\min}^2 \leq \|\mathbf{q}_k[n] - \mathbf{q}_i[n]\|^2, \forall k, i \in \mathcal{K}, i \neq k, \forall n, \quad (17c)$$

$$\|\mathbf{v}_k[n]\| \leq V_{\max}, \forall k, \forall n \in \mathcal{N} \setminus \{1\}, \quad (17d)$$

$$\alpha_{m,k}[n] \in \{0, 1\}, \forall m, k, n, \quad (17e)$$

$$\sum_{k \in \mathcal{K}} \alpha_{m,k}[n] = 1, \forall m, n, \quad (17f)$$

$$\{\omega_m^L[n], \omega_m^U[n], \omega_m^S[n]\} \in [0, 1], \forall m, n, \quad (17g)$$

$$\omega_m^L[n] + \omega_m^U[n] + \omega_m^S[n] = 1, \forall m, n, \quad (17h)$$

$$0 \leq f_m^L[n] \leq F_{\max}^L, \forall m, n, \quad (17i)$$

$$0 \leq f_{m,k}^U[n], \sum_{m \in \mathcal{M}} f_{m,k}^U[n] \leq F_{\max}^U, \forall m, k, n, \quad (17j)$$

$$0 \leq f_m^S[n], \sum_{m \in \mathcal{M}} f_m^S[n] \leq F_{\max}^S, \forall m, n, \quad (17k)$$

$$0 \leq p_{m,k}[n] \leq P_{\max}^U, \forall m, k, n, \quad (17l)$$

$$0 \leq p_{m,\text{LEO}}[n] \leq P_{\max}^S, \forall m, n, \quad (17m)$$

$$L_m^{\text{sum}}[n] \leq \tau, \forall n, m, \quad (17n)$$

$$\sum_{n \in \mathcal{N}} \left(E_k^{\text{prop}}[n] + \sum_{m \in \mathcal{M}} E_{m,k}^{\text{U,com}}[n] \right) \leq E_{\max}^{\text{UAV}}, \forall k, n, \quad (17o)$$

where F_{\max}^L , F_{\max}^U , and F_{\max}^S are the maximum computing frequencies of the MUs, the UAVs, and the LEO satellite, respectively. P_{\max}^U and P_{\max}^S denote the maximum transmit power of the MUs for communicating with the associated UAV, and the LEO satellite, respectively. E_{\max}^{UAV} denotes the energy budget of the UAVs. The constraints (17b)-(17d) represent the mobility constraints of the UAVs. The constraints (17e)-(17f) represent the association constraints among the MUs and the UAVs. The constraints (17g)-(17h) represent the task offloading decision constraints. The constraints (17i)-(17k) represent the constraints on the computing frequencies for local task processing, the computing frequencies for the UAV task processing, and the computing frequencies for the LEO satellite task processing. The constraints (17l)-(17m) represent the transmit power allocation from the MUs to the UAVs, and the transmit power allocation from the MUs to the LEO satellite. The constraint (17n) represents the latency constraint. Lastly, the constraint (17o) represents the constraint on the energy consumption of the UAVs.

In problem **P1**, the objective function $\frac{D_m[n]}{E_m^{\text{sum}}[n]}$ has a non-convex fractional expression involving multiple coupled vari-

ables and a binary variable. As a result, **P1** is a challenging mixed-integer nonlinear programming problem, which is difficult to be solved by conventional convex optimization methods.

IV. JOINT TRAJECTORY DESIGN, ASSOCIATION, AND RESOURCE ALLOCATION

In this section, we employ a quadratic transformation method to transfer the fractional structure in the objective function to decouple the numerators and denominators. We then decompose problem **P1** into four subproblems: the MU-UAV association, UAV trajectory optimization, task offloading decision, and transmit power control and CPU frequency control. The four subproblems are optimized in an alternate optimization manner.

A. Quadratic Transformation-based Problem Reformulation

Firstly, we employ a quadratic transformation method to reformulate the objective function.

Theorem 1. Given $M \times N$ pairs of non-negative functions $A_{m,n}(\mathbf{x}) : \mathbb{R}^d \rightarrow \mathbb{R}^+$ and positive functions $B_{m,n}(\mathbf{x}) : \mathbb{R}^d \rightarrow \mathbb{R}^{++}$, the sum-of-ratios problem

$$\max_{\{\mathbf{x}\}} \frac{1}{M} \frac{1}{N} \sum_{m=1}^M \sum_{n=1}^N \frac{A_{m,n}(\mathbf{x})}{B_{m,n}(\mathbf{x})} \quad (18a)$$

$$\text{s.t. } \mathbf{x} \in \mathcal{X}, \quad (18b)$$

is equivalent to

$$\max_{\{\mathbf{x}, \mathbf{y}\}} \frac{1}{M} \frac{1}{N} \sum_{m=1}^M \sum_{n=1}^N \left(2y_{m,n} \sqrt{A_{m,n}(\mathbf{x})} - y_{m,n}^2 B_{m,n}(\mathbf{x}) \right) \quad (19a)$$

$$\text{s.t. } \mathbf{x} \in \mathcal{X}, \quad (19b)$$

where \mathbf{x} is the variable, \mathcal{X} denotes the feasible set, \mathbf{y} represents the quadratic coefficients with size $M \times N$, and the m th row and the n th column of \mathbf{y} is $y_{m,n}$.

Proof. Please refer to [42]. \square

According to Theorem 1, problem **P1** can be transformed into the problem **P2**, which is shown as follows

$$\mathbf{P2:} \quad \max_{\{\mathbf{X}, \mathbf{y}\}} \sum_{m=1}^M \sum_{n=1}^N \left(2y_{m,n} \sqrt{D_m[n]} - y_{m,n}^2 E_m^{\text{sum}}[n] \right) \quad (20a)$$

$$\text{s.t. } (17b) - (17o), \quad (20b)$$

where $\mathbf{X} \triangleq \{\mathbf{Q}, \mathbf{P}, \mathbf{\Omega}, \mathbf{F}, \mathbf{\alpha}\}$, $\mathbf{y} = \{y_{m,n}, \forall m, n\}$ represents a matrix of size $M \times N$. In order to achieve the optimal energy efficiency, \mathbf{y} is updated alternately according to

$$y_{m,n} = \frac{\sqrt{D_m[n]}}{E_m^{\text{sum}}[n]}, \forall m, n, \quad (21)$$

and \mathbf{X} in problem **P2** is solved thereafter. Since each element in the matrix \mathbf{y} is non-decreasing after each iteration, it can be proved that the convergence is guaranteed.

The matrix \mathbf{y} is initialized with a small constant for each element. After that, we embark on a search for a feasible

solution set for \mathbf{X} . Subsequently, we update the value of each element in \mathbf{y} based on the obtained feasible \mathbf{X} . By repeating this process for a certain number of iterations, we can ultimately determine the optimal values of \mathbf{y}^* and \mathbf{X}^* .

B. Subproblem 1: MU-UAV Association Optimization

By fixing the variables $\mathbf{Q}, \mathbf{P}, \mathbf{\Omega}, \mathbf{F}$, the subproblem to optimize the MU-UAV association is formulated as

$$\mathbf{SP1:} \min_{\{\alpha\}} \sum_{m=1}^M \sum_{n=1}^N \alpha_{m,k}[n] y_{m,n}^2 \mathcal{W}_1[n] \quad (22a)$$

$$\text{s.t. (17e) - (17f), (17n) - (17o),} \quad (22b)$$

where

$$\begin{aligned} \mathcal{W}_1[n] = & \sum_{k \in \mathcal{K}} \frac{p_{m,k}[n] \omega_m^U[n] D_m[n]}{R_{m,k}[n]} \\ & + \sum_{k \in \mathcal{K}} \kappa_U (f_{m,k}^U[n])^2 \omega_m^U[n] D_m[n] \phi_m[n]. \end{aligned} \quad (23)$$

Problem **SP1** is a standard integer linear programming problem, which can be solved using conventional optimization methods, such as the branch-and-bound algorithm [43].

C. Subproblem 2: Task Offloading Decision Optimization

By fixing the variables $\mathbf{Q}, \mathbf{P}, \mathbf{F}, \alpha$, the subproblem to optimize the task offloading decision is formulated as

$$\mathbf{SP2:} \min_{\{\Omega\}} \sum_{m=1}^M \sum_{n=1}^N y_{m,n}^2 E_m^{\text{sum}}[n] \quad (24a)$$

$$\text{s.t. (17g) - (17h), (17n) - (17o),} \quad (24b)$$

where

$$\begin{aligned} E_m^{\text{sum}}[n] = & \omega_m^L[n] \mathcal{W}_2[n] + \omega_m^U[n] \mathcal{W}_3[n] + \omega_m^S[n] \mathcal{W}_4[n], \\ \mathcal{W}_2[n] = & \kappa_L (f_m^L[n])^2 D_m[n] \phi_m[n], \\ \mathcal{W}_3[n] = & \sum_{k=1}^K \alpha_{m,k}[n] \frac{p_{m,k}[n] D_m[n]}{R_{m,k}[n]} \\ & + \sum_{k=1}^K \alpha_{m,k}[n] \kappa_U (f_{m,k}^U[n])^2 D_m[n] \phi_m[n], \\ \mathcal{W}_4[n] = & \frac{p_{m,\text{LEO}}[n] D_m[n]}{R_{m,\text{LEO}}[n]} + \kappa_S (f_m^S[n])^2 D_m[n] \phi_m[n]. \end{aligned} \quad (25)$$

Problem **SP2** is a standard linear programming problem, which can be solved using the interior-point method [44].

D. Subproblem 3: Transmit Power Control and Computing Frequency Control Optimization

By fixing the variables $\mathbf{Q}, \mathbf{\Omega}, \alpha$, the subproblem to optimize the transmit power control and computing frequency control is formulated as

$$\mathbf{SP3:} \min_{\{\mathbf{P}, \mathbf{F}\}} \sum_{m=1}^M \sum_{n=1}^N y_{m,n}^2 E_m^{\text{sum}}[n] \quad (26a)$$

$$\text{s.t. (17i) - (17o).} \quad (26b)$$

where $E_m^{\text{sum}}[n] = \mathcal{W}_5[n] + \mathcal{W}_6[n]$, and given by

$$\begin{aligned} \mathcal{W}_5[n] = & \kappa_L (f_m^L[n])^2 \omega_m^L[n] D_m[n] \phi_m[n] \\ & + \kappa_S (f_m^S[n])^2 \omega_m^S[n] D_m[n] \phi_m[n] \\ & + \sum_{k \in \mathcal{K}} \alpha_{m,k}[n] \kappa_U (f_{m,k}^U[n])^2 \omega_m^U[n] D_m[n] \phi_m[n], \end{aligned} \quad (27)$$

$$\begin{aligned} \mathcal{W}_6[n] = & \frac{p_{m,\text{LEO}}[n] \omega_m^S[n] D_m[n]}{R_{m,\text{LEO}}[n]} \\ & + \sum_{k \in \mathcal{K}} \alpha_{m,k}[n] \frac{p_{m,k}[n] \omega_m^U[n] D_m[n]}{R_{m,k}[n]}. \end{aligned} \quad (28)$$

It is not difficult to verify that $\mathcal{W}_5[n]$ is a convex function with respect to variables $\{f_m^L[n], f_{m,k}^U[n], f_m^S[n]\}$. Furthermore, according to the following Proposition 1, we can conclude that $\mathcal{W}_6[n]$ is a concave function with respect to variables $\{p_{m,k}[n], p_{m,\text{LEO}}[n]\}$.

Proposition 1. *The function $\mathcal{W}_6[n]$ is a concave function with respect to variables $p_{m,k}[n]$, and $p_{m,\text{LEO}}[n]$.*

Proof. Please refer to Appendix A. \square

By introducing a set of auxiliary variables $\{\xi_{m,k}[n], \xi_{m,\text{LEO}}[n]\}$, $\mathcal{W}_6[n]$ can be approximated by

$$\begin{aligned} \tilde{\mathcal{W}}_6[n] = & \frac{\ln(2) \sigma_{\text{LEO}}^2 \omega_m^S[n] D_m[n]}{|g_{\text{LEO}}|^2 B_{\text{LEO}}} \xi_{m,\text{LEO}}[n] (e^{\frac{1}{\xi_{m,\text{LEO}}[n]}} - 1) \\ & + \sum_{k \in \mathcal{K}} \alpha_{m,k}[n] \frac{\ln(2) \sigma_{\text{UAV}}^2 \omega_m^U[n] D_m[n]}{h_{m,k}[n] B_{m,k}} \xi_{m,k}[n] (e^{\frac{1}{\xi_{m,k}[n]}} - 1), \end{aligned} \quad (29)$$

where $\xi_{m,k}[n]$ and $\xi_{m,\text{LEO}}[n]$ are given by

$$\xi_{m,k}[n] = \frac{1}{\ln \left(1 + \frac{p_{m,k}[n] h_{m,k}[n]}{\sigma_{\text{UAV}}^2} \right)}, \quad (30)$$

$$\xi_{m,\text{LEO}}[n] = \frac{1}{\ln \left(1 + \frac{p_{m,\text{LEO}}[n] |g_{\text{LEO}}|^2}{\sigma_{\text{LEO}}^2} \right)}. \quad (31)$$

Proposition 2. *The function $\tilde{\mathcal{W}}_6[n]$ is a convex function with respect to variables $\{\xi_{m,k}[n], \xi_{m,\text{LEO}}[n]\}$.*

Proof. Please refer to Appendix B. \square

It is worth noting that the directly expression of $\tilde{\mathcal{W}}_6[n]$ in CVX is not feasible. Therefore, we transfer it through the exponential cone optimization. Specifically, by introducing a set of auxiliary variables $\{\Gamma_{m,k}[n], \Gamma_{m,\text{LEO}}[n]\}$, $\tilde{\mathcal{W}}_6[n]$ can be rewritten as $\tilde{\mathcal{W}}_6'[n]$, and given by

$$\begin{aligned} \tilde{\mathcal{W}}_6'[n] = & \frac{\ln(2) \sigma_{\text{LEO}}^2 \omega_m^S[n] D_m[n]}{|g_{\text{LEO}}|^2 B_{\text{LEO}}} \Gamma_{m,\text{LEO}}[n] \\ & + \sum_{k \in \mathcal{K}} \alpha_{m,k}[n] \frac{\ln(2) \sigma_{\text{UAV}}^2 \omega_m^U[n] D_m[n]}{h_{m,k}[n] B_{m,k}} \Gamma_{m,k}[n], \end{aligned} \quad (32)$$

where

$$\xi_{m,\text{LEO}}[n] e^{\frac{1}{\xi_{m,\text{LEO}}[n]}} \leq \Gamma_{m,\text{LEO}}[n] + \xi_{m,\text{LEO}}[n], \quad (33)$$

$$\xi_{m,k}[n]e^{\frac{1}{\xi_{m,k}[n]}} \leq \Gamma_{m,k}[n] + \xi_{m,k}[n]. \quad (34)$$

Accordingly, we can rewrite constraints (17l)-(17n) as

$$\frac{1}{\ln\left(1 + \frac{P_{\max}^U h_{m,k}[n]}{\sigma_{\text{UAV}}^2}\right)} \leq \xi_{m,k}[n], \forall m, k, n, \quad (35)$$

$$\frac{1}{\ln\left(1 + \frac{P_{\max}^S |g_{\text{LEO}}|^2}{\sigma_{\text{LEO}}^2}\right)} \leq \xi_{m,\text{LEO}}[n], \forall m, n, \quad (36)$$

$$L_m^L[n] \leq \tau, \forall m, n, \quad (37)$$

$$L_m^U[n] = \sum_{k=1}^K \alpha_{m,k}[n] \frac{\ln(2)\omega_m^U[n]D_m[n]\xi_{m,k}[n]}{B_{m,k}} + \sum_{k=1}^K \alpha_{m,k}[n] \frac{\omega_m^U[n]D_m[n]\phi_m[n]}{f_{m,k}^U[n]} \leq \tau, \forall m, k, n, \quad (38)$$

$$L_m^S[n] = \frac{\ln(2)\omega_m^S[n]D_m[n]\xi_{m,\text{LEO}}[n]}{B_{\text{LEO}}} + \frac{\omega_m^S[n]D_m[n]\phi_m[n]}{f_m^S[n]} \leq \tau, \forall m, n. \quad (39)$$

To this end, the problem **SP3** is transformed into **SP3'**, which is written as

$$\mathbf{SP3'} \quad \min_{\{\mathbf{F}, \boldsymbol{\xi}, \boldsymbol{\Gamma}\}} \sum_{m=1}^M \sum_{n=1}^N y_{m,n}^2 (\mathcal{W}_5[n] + \tilde{\mathcal{W}}'_6[n]) \quad (40a)$$

$$\text{s.t. (17i) - (17k), (17o), (33) - (39), \quad (40b)$$

where $\boldsymbol{\xi} = \{\xi_{m,k}[n], \xi_{m,\text{LEO}}[n], \forall m, k, n\}$, $\boldsymbol{\Gamma} = \{\Gamma_{m,k}[n], \Gamma_{m,\text{LEO}}[n], \forall m, k, n\}$. The problem **SP3'** is a convex optimization problem, which can be solved by CVX.

E. Subproblem 4: UAV Trajectory Optimization

By fixing the variables $\mathbf{P}, \boldsymbol{\Omega}, \mathbf{F}, \boldsymbol{\alpha}$, the subproblem to optimize the UAV trajectory is formulated as

$$\mathbf{SP4}: \min_{\{\mathbf{Q}\}} \sum_{m=1}^M \sum_{n=1}^N y_{m,n}^2 E_m^{\text{U,tran}}[n] \quad (41a)$$

$$\text{s.t. (17b) - (17d), (17n) - (17o). \quad (41b)$$

Regarding the inequality constraint (17o), $E_k^{\text{prop}}[n]$ contains $\frac{\zeta_2}{\|\mathbf{v}_k[n]\|}$, which is a reciprocal of a convex function. Therefore, the constraint (17o) is a non-convex constraint. To address this, we introduce an auxiliary variable $\psi_k[n]$, which satisfies

$$\psi_k^2[n] \leq \frac{\|\mathbf{q}_k[n] - \mathbf{q}_k[n-1]\|^2}{\tau^2}. \quad (42)$$

Therefore, $E_k^{\text{prop}}[n]$ can be approximated by its convex upper bound

$$\hat{E}_k^{\text{prop}}[n] = \tau \left(\zeta_1 \|\mathbf{v}_k[n]\|^3 + \frac{\zeta_2}{\psi_k[n]} \right). \quad (43)$$

By replacing $E_k^{\text{prop}}[n]$ with $\hat{E}_k^{\text{prop}}[n]$, the inequality constraint (17o) can be transformed into

$$\sum_{n \in \mathcal{N}} \left(\hat{E}_k^{\text{prop}}[n] + \sum_{m \in \mathcal{M}} E_{m,k}^{\text{U,com}}[n] \right) \leq E_{\max}^{\text{UAV}}. \quad (44)$$

Moreover, the constraint (42) is non-convex. We convert it into the following convex form via the successive convex approximation (SCA) method [30], [45], which is given by

$$\psi_k^2[n]\tau^2 \leq \|\mathbf{q}_k^{(l)} - \mathbf{q}_k^{(l)}[n-1]\|^2 + 2(\mathbf{q}_k^{(l)}[n] - \mathbf{q}_k^{(l)}[n-1])^\top (\mathbf{q}_k[n] - \mathbf{q}_k[n-1]). \quad (45)$$

Similarly, the constraint (17c) can be transformed as

$$d_{\min}^2 \leq -\|\mathbf{q}_k^{(l)}[n] - \mathbf{q}_i^{(l)}[n]\|^2 + 2(\mathbf{q}_k^{(l)}[n] - \mathbf{q}_i^{(l)}[n])^\top (\mathbf{q}_k[n] - \mathbf{q}_i[n]). \quad (46)$$

As for constraint (17n), only $L_m^U[n]$ is related to the UAV trajectory. Thus, we mainly consider the equivalent constraint $L_m^U[n] \leq \tau$. By introducing auxiliary variables $S_{m,k}[n]$ and $\gamma_{m,k}[n] = R_{m,k}[n]$, where $S_{m,k}[n]$ and $\gamma_{m,k}[n]$ satisfy

$$S_{m,k}[n] \leq H^2 + \|\mathbf{q}_k[n] - \mathbf{s}_m[n]\|^2, \quad (47)$$

$$\gamma_{m,k}[n] \leq B_{m,k} \log_2 \left(1 + \frac{p_{m,k}[n]\beta_0}{S_{m,k}[n]\sigma_{\text{UAV}}^2} \right), \quad (48)$$

$L_m^U[n] \leq \tau$ can be transformed as

$$\sum_{k=1}^K \alpha_{m,k}[n] \left(\frac{\omega_m^U[n]D_m[n]}{\gamma_{m,k}[n]} + \frac{\omega_m^U[n]D_m[n]\phi_m[n]}{f_{m,k}^U[n]} \right) \leq \tau. \quad (49)$$

It is easy to prove that $B_{m,k} \log_2 \left(1 + \frac{p_{m,k}[n]\beta_0}{S_{m,k}[n]\sigma_{\text{UAV}}^2} \right)$ is convex with respect to $S_{m,k}[n]$. Then, similar to the transformation in (45), the constraint (49) can be converted into

$$\gamma_{m,k}[n] \leq B_{m,k} \left(\log_2 (S_{m,k}[n]\sigma_{\text{UAV}}^2 + p_{m,k}[n]\beta_0) - \log_2 (S_{m,k}^l[n]\sigma_{\text{UAV}}^2) - \frac{\log_2(e)}{S_{m,k}^l[n]} (S_{m,k}[n] - S_{m,k}^l[n]) \right). \quad (50)$$

Similarly, the constraint $S_{m,k}[n] \leq H^2 + \|\mathbf{q}_k[n] - \mathbf{s}_m[n]\|^2$ can be transformed as

$$S_{m,k}[n] \leq \|\mathbf{q}_k^l[n] - \mathbf{s}_m[n]\|^2 + H^2 + 2(\mathbf{q}_k^l[n] - \mathbf{s}_m[n])^\top (\mathbf{q}_k[n] - \mathbf{q}_k^l[n]). \quad (51)$$

Then, the objective function is written as

$$\Upsilon_m[n] = y_{m,n}^2 E_m^{\text{U,tran}}[n] = y_{m,n}^2 \sum_{k=1}^K \alpha_{m,k}[n] \frac{p_{m,k}[n]\omega_m^U[n]D_m[n]}{\gamma_{m,k}[n]}. \quad (52)$$

To this end, the problem **SP4** is transformed into the following **SP4'**, which is written as

$$\mathbf{SP4'}: \min_{\{\mathbf{Q}, \boldsymbol{\psi}, \boldsymbol{\gamma}, \mathbf{S}\}} \sum_{m=1}^M \sum_{n=1}^N \Upsilon_m[n] \quad (53a)$$

$$\text{s.t. (17b), (17d), (44) - (46), (49) - (51), \quad (53b)$$

where $\boldsymbol{\psi} = \{\psi_k[n], \forall k, n\}$, $\boldsymbol{\gamma} = \{\gamma_{m,k}[n], \forall m, k, n\}$, $\mathbf{S} = \{S_{m,k}[n], \forall m, k, n\}$. The problem **SP4'** is a convex optimization problem, which can be solved by CVX.

F. Overall Algorithm and Complexity Analysis

The AO-based algorithm for solving problem **P1** is detailed in Algorithm 1, which alternately optimizes the MU-UAV association, UAV trajectory, task offloading decision, and transmit power control and CPU frequency control in an iterative manner until the objective value converges or the maximum iteration number is reached.

Algorithm 1 AO-based Algorithm for Solving **P1**

Input: An initial feasible point $\{Q^0, P^0, \Omega^0, F^0, \alpha^0\}$;
Initialize: Iteration number $l = 0$, precision threshold ε , and number of maximum iterations l_{\max} ;
 Compute the initial quadratic transform variable $y_{m,n}^0$ according to (21) and the initial objective function value, i.e. $\Phi^0(Q^0, P^0, \Omega^0, F^0, \alpha^0)$;
repeat
 Solve the problem **SP1** to get the MU-UAV association α^{l+1} for given Q^l, P^l, Ω^l, F^l ;
 Solve the problem **SP2** to get the task offloading decision Ω^{l+1} for given $Q^l, P^l, F^l, \alpha^{l+1}$;
 Solve the problem **SP3** to get the transmit power control and CPU frequency control P^{l+1}, F^{l+1} for given $Q^l, \Omega^{l+1}, \alpha^{l+1}$;
 Solve the problem **SP4** to get the UAV trajectory Q^{l+1} for given $P^{l+1}, \Omega^{l+1}, F^{l+1}, \alpha^{l+1}$;
 Update the quadratic transform variable $y_{m,n}^{l+1}$ according to (21);
 Update the objective function value according to above variables, i.e. $\Phi(Q^{l+1}, P^{l+1}, \Omega^{l+1}, F^{l+1}, \alpha^{l+1})$;
 Update $l = l + 1$;
until The objective function between two adjacent iterations is smaller than precision threshold ε or $l > l_{\max}$;
Output: Φ^* ($Q^*, P^*, \Omega^*, F^*, \alpha^*$), Q^* , P^* , Ω^* , F^* , and α^* .

1) *Convergence Analysis:* Similar to the notations in Algorithm 1, we define Q^l, P^l, Ω^l, F^l , and α^l as the solution in the l th iteration. The objective function is defined as $\Phi(Q^l, P^l, \Omega^l, F^l, \alpha^l)$. Thus, we have

$$\begin{aligned} \Phi(Q^l, P^l, \Omega^l, F^l, \alpha^l) &\leq \Phi(Q^l, P^l, \Omega^l, F^l, \alpha^{l+1}) \\ &\leq \Phi(Q^l, P^l, \Omega^{l+1}, F^l, \alpha^{l+1}) \\ &\leq \Phi(Q^l, P^{l+1}, \Omega^{l+1}, F^{l+1}, \alpha^{l+1}) \\ &\leq \Phi(Q^{l+1}, P^{l+1}, \Omega^{l+1}, F^{l+1}, \alpha^{l+1}), \end{aligned} \quad (54)$$

which shows that the value of the objective function is non-decreasing over iterations. In addition, the energy efficiency is bounded due to the finite range of the optimization variables. Therefore, Algorithm 1 is guaranteed to converge.

2) *Complexity Analysis:* In Algorithm 1, we solve the subproblem **SP1** using the binary cut-and-branch method [43], and solve other subproblems using the interior point method [44]. Thus, the computational complexity of the four subproblems are $\mathcal{O}(MKN \log(MKN))$, $\mathcal{O}((MN)^{3.5} \log(1/\epsilon))$, $\mathcal{O}((MKN)^{3.5} \log(1/\epsilon))$, $\mathcal{O}((MKN)^{3.5} \log(1/\epsilon))$, respectively, where ϵ represents the tolerance. Consequently, the complexity of Algorithm 1 is $\mathcal{O}(\mathcal{I}(((MN)^{3.5} + (MKN)^{3.5} + (MKN)^{3.5}) \log(1/\epsilon) + MKN \log(MKN)))$, where \mathcal{I} denotes the iteration number.

V. NUMERICAL RESULTS

In the simulations, we consider $K = 2$ UAVs fly from specified initial positions to specified final positions to provide

computing services for the MUs. We consider $M = 8$ MUs that are randomly distributed in a square area of $1000 \times 1000 \text{ m}^2$. All UAVs fly at a height of 100 m. Unless otherwise stated, the remaining simulation parameters are summarized in Table ?? [46].

TABLE I: Simulation Parameters.

Parameters	Value
Task period, T	40 s
Number of time slot, N	40
Duration of time slot, τ	1 s
Minimum secure distance, d_{\min}	50 m
Maximum speed, V_{\max}	50 m/s
UAV's propulsion parameters, ζ_1, ζ_2	0.00614, 15.976
Channel power gain between the UAVs and the MUs, β_0	-60 dBm
Noise power at the UAV, σ_{UAV}	-170 dBm
Channel power gain between the LEO satellite and the MUs, g_{LEO}	[5,10] dBm
Noise power at the LEO satellite, σ_{LEO}	-170 dBm
Maximum transmit power, P_{\max}	3 w
Data size, $D_m[n]$	[5.5, 6.5] Mbits
Computing cycles for 1-bit data, $\phi_m[n]$	100 cycles/bit
MU maximum computing frequency, F_{\max}^L	5 Ghz
MU computing capacitance coefficient, κ_L	10^{-26}
UAV maximum computing frequency, F_{\max}^U	9 Ghz
UAV computing capacitance coefficient, κ_U	10^{-27}
LEO satellite maximum computing frequency, F_{\max}^S	9 Ghz
LEO satellite computing capacitance coefficient, κ_S	10^{-27}

To evaluate the performance and efficiency of the proposed scheme, we compare it with four baseline schemes, which are given in the following.

- 1) *Single UAV Scheme:* The considered SAGIN system has only one UAV that can provide computing services for the MUs.
- 2) *Fixed Trajectory Scheme:* The trajectories of the UAVs are fixed.
- 3) *Fixed Allocation Scheme:* The task offloading decisions of the MUs are fixed.
- 4) *LS Offloading Scheme:* Only the LEO satellite provides computing services for the MUs.

As shown in Fig. 2, we present the total energy efficiency under different schemes with respect to the number of iterations. The results clearly show that the total energy efficiency initially exhibits a significant increase, followed by a gradual convergence to a stable value as the number of iterations progresses, which validates the convergence of all schemes. Notably, the total energy efficiency of the proposed scheme is the highest among all schemes, which can be attributed to the joint design of the MU-UAV association, UAV trajectory, task offloading decision, transmit power control, and CPU frequency control.

Fig. 3 and Fig. 4 respectively illustrate the optimized trajectories of the UAVs under the single UAV scheme and the proposed scheme. It can be observed that the UAV trajectories consistently tend towards regions densely populated with the MUs. This proximity typically enhances the transmission rates between the MUs and the UAVs, thereby improving the timelines of service responses. Further, the comparative

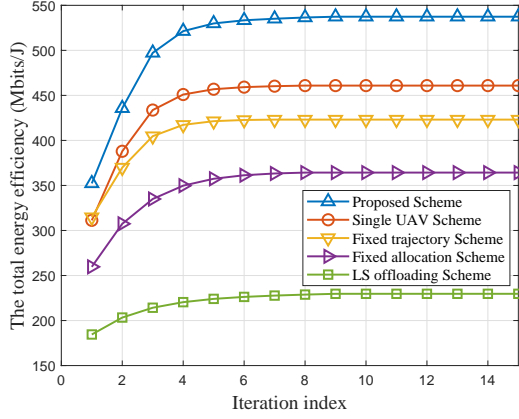


Fig. 2: The total energy efficiency under different schemes versus the number of iterations.

analysis of Fig. 3 and Fig. 4 reveals that as the number of the UAVs increases, the number of the MUs served by each UAV decreases. This enables the UAVs to more effectively optimize their positions to approach the MUs they serve, leading to a substantial improvement in the transmission rates between the UAVs and the MUs they serve.

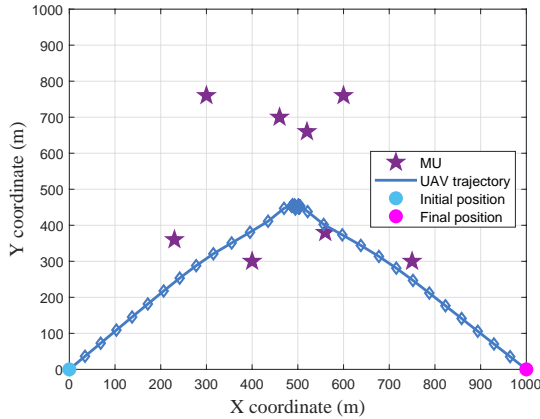


Fig. 3: The optimized trajectory of the UAV under the single UAV scheme.

Fig. 5 and Fig. 6 show that, as the number of MUs increases, our proposed scheme exhibits a more significant increase in total energy efficiency compared to other four schemes, while the increase in energy consumption is relatively smaller. The reason can be explained as follows. As the number of MUs grows, the demand for the UAV services increases, and the various schemes exhibit different levels of adaptability to these changes. Specifically, the single UAV scheme deploys only a single UAV, which makes it challenging to ensure high-quality communication services for every MU when a large number of MUs require for the services. The fixed trajectory scheme lacks flexibility, especially when there are multiple UAVs. This means that in scenarios with the uneven MU distribution or dynamic demand changes, the scheme struggles to optimize service quality by adjusting the UAV positions. The fixed

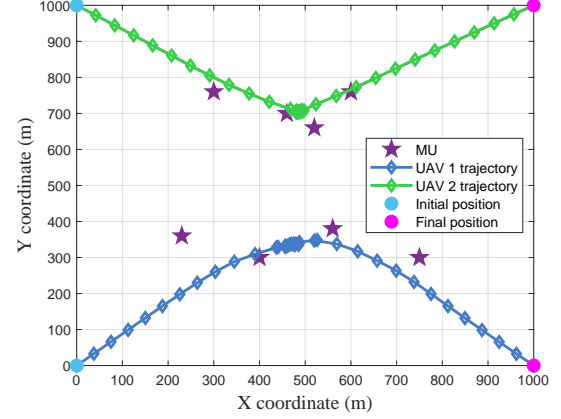


Fig. 4: The optimized trajectories of the UAVs under the proposed scheme.

allocation scheme employs a fixed task allocation decision, which means it cannot adjust the allocation of tasks based on real-time network conditions. In contrast, our scheme dynamically reallocates tasks according to the current network state, ensuring higher service quality and better user experience. The LS offloading scheme relies solely on local computing resources and the LEO satellite assisted computing without considering the role of the UAVs. Although this approach can provide a certain level of service, the absence of the UAV support makes it difficult to achieve ideal computational quality and efficiency in scenarios with a large-scale MU distribution. Therefore, under the same number of MUs, our proposed scheme demonstrates the best performance. Specifically, from the numerical results, when the number of the MUs is 16, our proposed scheme outperforms the single UAV scheme, fixed trajectory scheme, fixed allocation scheme, and LS offloading scheme by 17.53%, 22.55%, 48.27%, and 133.90%, respectively, in terms of the overall computational energy efficiency.

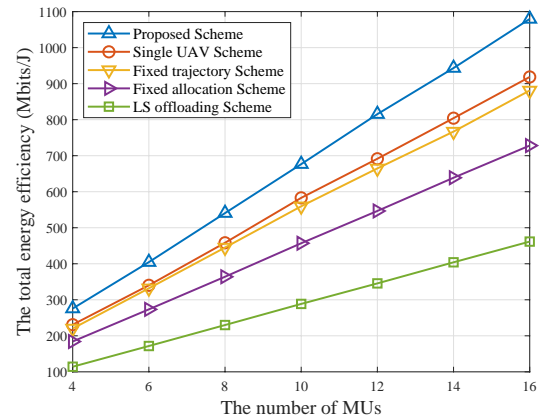


Fig. 5: The total energy efficiency versus the number of MUs.

Fig. 7 and Fig. 8 show that, as the amount of task data that the MUs need to process per time slot increases, the total energy efficiency of all schemes decreases, and the

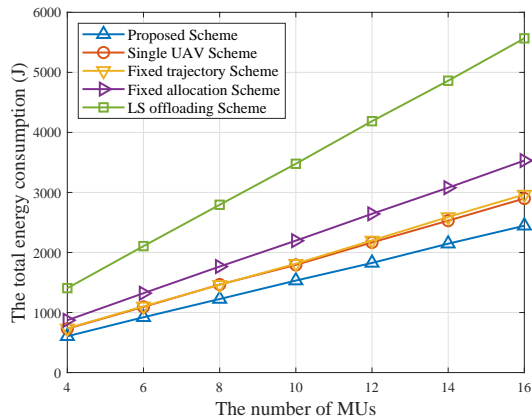


Fig. 6: The total energy consumption versus the number of MUs.

required energy consumption also increases. Notably, in both key metrics of total energy efficiency and energy consumption, our proposed algorithm outperforms other four algorithms. The reason is that as the amount of task data increases, the MUs tend to offload more tasks to the UAVs and the LEO satellite for remote computing, leading to an increase in communication energy consumption, which in turn reduces the total energy efficiency of all schemes. Moreover, the LS offloading scheme experiences the most significant increase in total energy consumption, and the rate of increase is notably faster than that of other four schemes. The reason is that, in the LS offloading scheme, the MUs do not offload tasks to the UAVs.

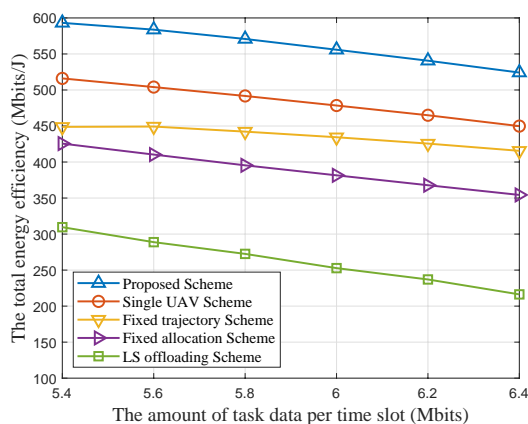


Fig. 7: The total energy efficiency versus the amount of task data per time slot.

Fig. 9 presents the total computational energy efficiency versus the communication bandwidth between the UAVs and the MUs. It can be observed that the total energy efficiency significantly increases with the growth of the communication bandwidth between the MUs and the UAVs for the proposed scheme, single UAV scheme, and fixed trajectory scheme, whereas the increase is relatively slower for fixed allocation scheme, and remains unchanged for LS offloading scheme.

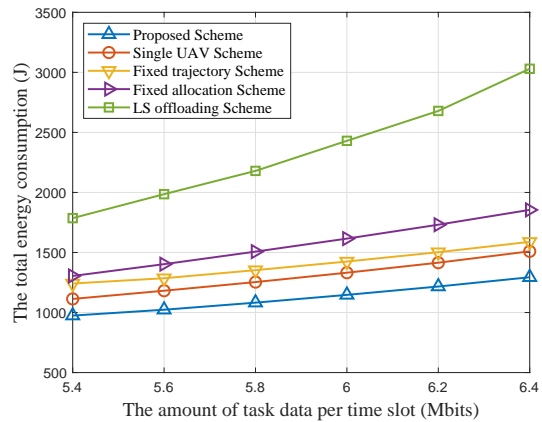


Fig. 8: The total energy consumption versus the amount of task data per time slot.

The reason is that the increase in communication bandwidth enhances the task transmission rate between the MUs and the UAVs, allowing the UAVs to assist in processing a larger volume of tasks within each time slot τ . Specifically, for the proposed scheme, single UAV scheme, and fixed trajectory scheme, the increase in communication bandwidth means that the MUs can offload tasks to the UAVs more quickly, improving the efficiency of task processing and reducing the burden of local computation, thus enhancing overall energy efficiency. However, in the fixed allocation scheme, since the proportions of task offloading to the UAVs is fixed, the growth in communication bandwidth can only reduce the energy consumption associated with the UAV computing, but does not enable the MUs to offload more tasks to the UAV, thereby limiting its potential for improvement in energy efficiency. For the LS offloading scheme, since there is no UAV involved, the increase in communication bandwidth has no effect, and the total energy efficiency remains a constant.

Fig. 10 presents the total energy consumption versus the communication bandwidth between the UAVs and the MUs. The proposed scheme, single UAV scheme, and fixed trajectory scheme demonstrate a significant reduction in total energy consumption as the communication bandwidth increases, whereas the reduction is relatively slower for the fixed allocation scheme, and remains unchanged for the LS offloading scheme. The reason is that the increase in communication bandwidth significantly enhances the communication rate between the MUs and the UAVs, thereby increasing the proportion of tasks offloaded from the MUs to the UAVs, which is shown in Fig. 11. Specifically, when the communication bandwidth increases from 1 MHz to 2 MHz, the average proportion of tasks offloaded to the UAVs rises from 49% to 65%, while the average proportion of tasks processed locally decreases from 31% to 24% in the proposed scheme. Since the MUs are equipped with low energy-efficient processors, offloading more tasks to the UAVs for processing can effectively lower the total energy consumption of the system.

From Fig. 12, we can observe that the amount of task data offloaded to the UAVs initially increases gradually, then stabi-

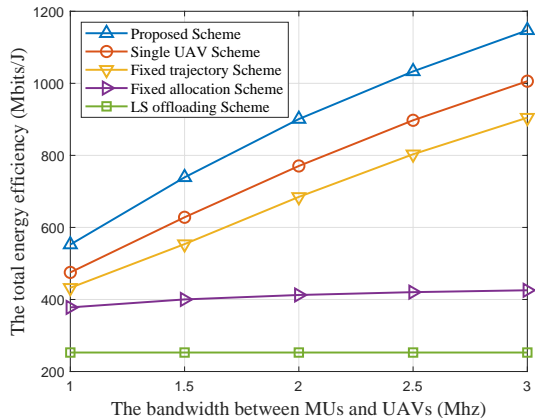


Fig. 9: The total computational energy efficiency versus the bandwidth of UAVs.

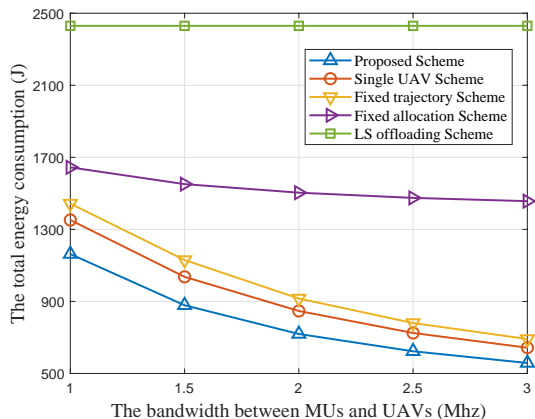


Fig. 10: The total energy consumption versus the bandwidth of UAVs.

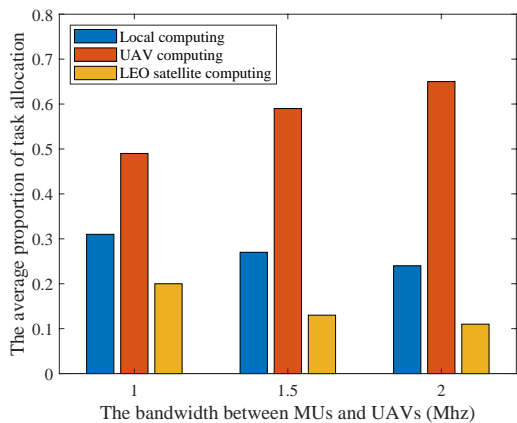


Fig. 11: Task allocation at different communication bandwidth.

lizes, and finally decreases as time elapses. This phenomenon is attributed to the channel gains between the UAVs and the MUs. In the initial time slot, the UAVs move towards the area with higher MU density. During this movement, as the UAVs approach the MUs, the communication rates between the MUs and the UAVs increase, leading to a corresponding increase in the size of tasks offloaded to the UAVs. Between the time slots 11 and 29, the amount of task data offloaded to the UAVs generally remains a constant. The reason is that during this period, the UAVs are hovering near the area with high MU density, maintaining a high communication rate, which keeps the level of task offloading stable. As the index of the time slot continues to increase, the UAVs move near to the final position, causing a decrease in the communication rates between the UAVs and the MUs, which in turn reduces the amount of task data offloaded to the UAVs. Meanwhile, the amount of task data processed locally by the MUs and the amount of task data offloaded to the LEO satellite exhibit a divergent trend from that of the UAVs. This trend reflects adaptive task offloading decisions in response to changes in the UAVs' position and communication conditions, aiming to maximize the overall energy efficiency.

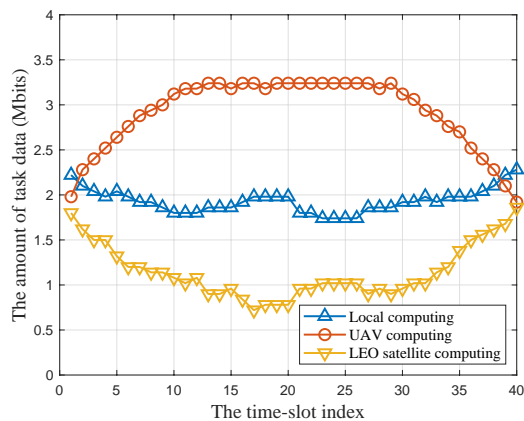


Fig. 12: Task allocation at each slot.

VI. CONCLUSION

In this paper, we design a multi-UAV enabled SAGIN with MEC, aiming to provide efficient computing services for the MUs. Specifically, under the constraints of task delay and UAV energy limitations, we formulate a joint optimization problem targeting the maximization of the total energy efficiency. The problem involves optimizing the UAV trajectories, the MU-UAV association, the task offloading decision, the computing frequency, and the transmission power control. To solve the problem, we decompose it into four subproblems and propose an effective AO-based algorithm. Additionally, we conduct detailed analysis of the convergence and computational complexity of the proposed algorithm. Numerical results demonstrate that our proposed scheme significantly outperforms other benchmark schemes. These results confirm that our scheme not only effectively improves the computational energy efficiency of the system, but also meets the computational demands of the MUs, particularly in scenarios with high number of MUs.

APPENDIX A
THE PROOF OF PROPOSITION 1

Proof. Define a function $F(x) = \frac{Ax}{\ln(1+Bx)}$, with $x \geq 0$, and $A > 0$, $B > 0$ are two constants. First, we prove the non-convexity of the function $F(x)$. The second-order derivatives of $F(x)$ with regard to x is

$$\frac{d^2F(x)}{dx^2} = \frac{2AB^2x - (AB^2x + 2AB)\ln(1+Bx)}{(1+Bx)^2\ln^3(1+Bx)}. \quad (55)$$

Let $G(x) = 2AB^2x - (AB^2x + 2AB)\ln(1+Bx)$, the first-order derivative and second-order derivative of $G(x)$ with regard to x are

$$\frac{dG(x)}{dx} = \frac{AB^3x}{1+Bx} - AB^2\ln(1+Bx), \quad (56)$$

$$\frac{d^2G(x)}{dx^2} = -\frac{AB^4x}{(1+Bx)^2}. \quad (57)$$

Clearly, $\frac{d^2G(x)}{dx^2} \leq 0$. Thus, $\frac{dG(x)}{dx}$ is a monotonically non-increasing function, and $\frac{dG(x)}{dx} \leq \frac{dG(x)}{dx}|_{x=0} = 0$. Consequently, $G(x) \leq G(0) = 0$. Thus, $\frac{d^2F(x)}{dx^2} \leq 0$, indicating that $F(x)$ is a concave function with respect to x .

Let A , B be $\sum_{k \in \mathcal{K}} \alpha_{m,k}[n] \frac{\omega_m^U[n] D_m[n] \ln(2)}{B_{m,k}}$, $\frac{h_{m,k}[n]}{\sigma_{AV}^2}$, respectively. By replacing x with $p_{m,k}[n]$, we conclude that the function $\mathcal{W}_6[n]$ is non-convex with respect to $p_{m,k}[n]$. Similarly, we can also conclude that the function $\mathcal{W}_6[n]$ is concave with respect to $p_{m,LEO}[n]$. This proof is completed. \square

APPENDIX B
THE PROOF OF PROPOSITION 2

Proof. Define $H(x) = Ax(e^{\frac{1}{x}} - 1)$, with $x > 0$, and $A > 0$ is constants. Since

$$\frac{d^2H(x)}{dx^2} = \frac{e^{\frac{1}{x}}}{x^3} > 0, \quad (58)$$

one can get that $H(x)$ is a convex function with respect to x .

Let $A = \alpha_{m,k}[n] \frac{\ln(2)\sigma_{AV}^2\omega_m^U[n]D_m[n]}{h_{m,k}[n]B_{m,k}}$, and $x = \xi_{m,k}[n]$, $\frac{\partial^2\mathcal{W}_6[n]}{\partial\xi_{m,k}^2[n]} > 0$ can be obtained. Thus $\mathcal{W}_6[n]$ is a convex function with respect to variables $\xi_{m,k}[n]$. Similarly, $\frac{\partial^2\mathcal{W}_6[n]}{\partial\xi_{m,LEO}^2[n]} > 0$ can also be obtained, and $\mathcal{W}_6[n]$ is a convex function with respect to variables $\xi_{m,LEO}[n]$. This proof is completed. \square

REFERENCES

- [1] J. Liu, Y. Shi, Z. M. Fadlullah, and N. Kato, "Space-air-ground integrated network: A survey," *IEEE Commun. Surveys Tuts.*, vol. 20, no. 4, pp. 2714–2741, 4th Quart. 2018.
- [2] S. Zhang, A. Liu, C. Han, X. Liang, X. Xu, and G. Wang, "Multiagent reinforcement learning-based orbital edge offloading in SAGIN supporting internet of remote things," *IEEE Internet Things J.*, vol. 10, no. 23, pp. 20472–20483, Dec. 2023.
- [3] H. Wang, X. Xia, T. Song, and Y. Xing, "Survey on space-air-ground integrated networks in 6G," in *Proc. IEEE/CIC Int. Conf. Commun. China, ICC C Workshops*, Xiamen, China, Jul. 2021, pp. 315–320.
- [4] J. Liu, X. Du, J. Cui, M. Pan, and D. Wei, "Task-oriented intelligent networking architecture for the space-air-ground-aqua integrated network," *IEEE Internet Things J.*, vol. 7, no. 6, pp. 5345–5358, Jun. 2020.
- [5] M. Hosseinian, J. P. Choi, S.-H. Chang, and J. Lee, "Review of 5G NTN standards development and technical challenges for satellite integration with the 5G network," *IEEE Aerosp. Electron. Syst. Mag.*, vol. 36, no. 8, pp. 22–31, Aug. 2021.

- [6] T. X. Tran, A. Hajisami, P. Pandey, and D. Pompili, "Collaborative mobile edge computing in 5G networks: New paradigms, scenarios, and challenges," *IEEE Commun. Mag.*, vol. 55, no. 4, pp. 54–61, Apr. 2017.
- [7] X. Wang, H. Chen, and F. Tan, "Hybrid OMA/NOMA mode selection and resource allocation in space-air-ground integrated networks," *IEEE Trans. Veh. Technol.*, to appear, 2024.
- [8] Q. Wu, Y. Zeng, and R. Zhang, "Joint trajectory and communication design for multi-UAV enabled wireless networks," *IEEE Trans. Wireless Commun.*, vol. 17, no. 3, pp. 2109–2121, Mar. 2018.
- [9] M. N. Dazhi, H. Al-Hraishawi, B. Shankar, and S. Chatzinotas, "Terminal-aware multi-connectivity scheduler for uplink multi-layer non-terrestrial networks," in *Proc. IEEE Glob. Commun. Conf., GLOBECOM Workshops*, Virtual, Brazil, Dec. 2022, pp. 1133–1139.
- [10] A. Bakambekova, N. Kouzayha, and T. Al-Naffouri, "On the interplay of artificial intelligence and space-air-ground integrated networks: A survey," *IEEE Open J. Commun. Soc.*, vol. 5, pp. 4613–4673, Jul. 2024.
- [11] Y. Liu, L. Jiang, Q. Qi, and S. Xie, "Energy-efficient space-air-ground integrated edge computing for internet of remote things: A federated DRL approach," *IEEE Internet Things J.*, vol. 10, no. 6, pp. 4845–4856, Mar. 2023.
- [12] S. Zhang, N. Yi, and Y. Ma, "A survey of computation offloading with task types," *IEEE Trans. Intell. Transp. Syst.*, vol. 25, no. 8, pp. 8313–8333, Aug. 2024.
- [13] Y. Mao, C. You, J. Zhang, K. Huang, and K. B. Letaief, "A survey on mobile edge computing: The communication perspective," *IEEE Commun. Surveys Tuts.*, vol. 19, no. 4, pp. 2322–2358, 4th Quart. 2017.
- [14] P. Mach and Z. Becvar, "Mobile edge computing: A survey on architecture and computation offloading," *IEEE Commun. Surveys Tuts.*, vol. 19, no. 3, pp. 1628–1656, 3rd Quart. 2017.
- [15] Q. Chen, W. Meng, S. Han, C. Li, and H. H. Chen, "Effect of intelligent multi-association in civil aircraft-augmented SAGIN," *IEEE Trans. on Cogn. Commun. Netw.*, vol. 9, no. 1, pp. 223–238, Feb. 2023.
- [16] X. Wang, L. T. Yang, D. Meng, M. Dong, K. Ota, and H. Wang, "Multi-UAV cooperative localization for marine targets based on weighted subspace fitting in SAGIN environment," *IEEE Internet Things J.*, vol. 9, no. 8, pp. 5708–5718, Apr. 2022.
- [17] E. M. Mohamed, M. Ahmed Alnakhli, and M. M. Fouda, "Joint UAV trajectory planning and LEO-sat selection in SAGIN," *IEEE Open J. Commun. Soc.*, vol. 5, pp. 1624–1638, 2024.
- [18] F. Tang, H. Hofner, N. Kato, K. Kaneko, Y. Yamashita, and M. Hangai, "A deep reinforcement learning-based dynamic traffic offloading in space-air-ground integrated networks (SAGIN)," *IEEE J. Sel. Areas Commun.*, vol. 40, no. 1, pp. 276–289, Jan. 2022.
- [19] Q. Liu, M. Fu, W. Li, J. Xie, and M. Kadoch, "RIS-assisted ambient backscatter communication for SAGIN IoT," *IEEE Internet Things J.*, vol. 10, no. 11, pp. 9375–9384, Jun. 2023.
- [20] F. Tang, C. Wen, L. Luo, M. Zhao, and N. Kato, "Blockchain-based trusted traffic offloading in space-air-ground integrated networks (SAGIN): A federated reinforcement learning approach," *IEEE J. Sel. Areas Commun.*, vol. 40, no. 12, pp. 3501–3516, Dec. 2022.
- [21] W. Liu, J. Wang, H. Xing, Z. Jin, X. Zhang, and Y. Shen, "Blockchain-empowered space-air-ground integrated networks for remote internet of things," in *Proc. IEEE/CIC Int. Conf. Commun. China, ICC C*, Dalian, China, Aug. 2023, pp. 1–6.
- [22] H. Jia, Y. Wang, and W. Wu, "Dynamic resource allocation for remote IoT data collection in sagin," *IEEE Internet Things J.*, vol. 11, no. 11, pp. 20575–20589, Jun. 2024.
- [23] X. Meng, N. Zhang, M. Jian, M. Kadoch, and D. Yang, "Channel modeling and estimation for reconfigurable-intelligent-surface-based 6G SAGIN IoT," *IEEE Internet Things J.*, vol. 10, no. 11, pp. 9273–9282, Jun. 2023.
- [24] J. Ren, G. Yu, Y. Cai, and Y. He, "Latency optimization for resource allocation in mobile-edge computation offloading," *IEEE Trans. Wireless Commun.*, vol. 17, no. 8, pp. 5506–5519, Aug. 2018.
- [25] J. Ren, G. Yu, Y. He, and G. Y. Li, "Collaborative cloud and edge computing for latency minimization," *IEEE Trans. Veh. Technol.*, vol. 68, no. 5, pp. 5031–5044, May 2019.
- [26] X. Cao, F. Wang, J. Xu, R. Zhang, and S. Cui, "Joint computation and communication cooperation for energy-efficient mobile edge computing," *IEEE Internet Things J.*, vol. 6, no. 3, pp. 4188–4200, Jun. 2019.
- [27] F. Wang, J. Xu, and S. Cui, "Optimal energy allocation and task offloading policy for wireless powered mobile edge computing systems," *IEEE Trans. Wireless Commun.*, vol. 19, no. 4, pp. 2443–2459, Apr. 2020.
- [28] X. Zhang, Y. Shen, B. Yang, W. Zang, and S. Wang, "DRL based data offloading for intelligent reflecting surface aided mobile edge

- computing,” in *Proc. IEEE Wireless Commun. Netw. Conf., WCNC*, Nanjing, China, Mar. 2021, pp. 1–7.
- [29] B. Liang, R. Fan, H. Hu, H. Jiang, J. Xu, and N. Zhang, “Joint task offloading and resource allocation in multi-user mobile edge computing with continuous spectrum sharing,” *IEEE Trans. Veh. Technol.*, vol. 73, no. 5, pp. 7234–7249, May 2024.
- [30] W. Liu, H. Wang, X. Zhang, H. Xing, J. Ren, Y. Shen, and S. Cui, “Joint trajectory design and resource allocation in UAV-enabled heterogeneous MEC systems,” *IEEE Internet Things J.*, to appear, 2024.
- [31] C. Chen, S. Gong, W. Zhang, Y. Zheng, and Y. C. Kiat, “Drl-based contract incentive for wireless-powered and uav-assisted backscattering mec system,” *IEEE Trans. on Cloud Comput.*, vol. 12, no. 1, pp. 264–276, Jan.-Mar. 2024.
- [32] C. Huang, G. Chen, P. Xiao, Y. Xiao, Z. Han, and J. A. Chambers, “Joint offloading and resource allocation for hybrid cloud and edge computing in SAGINs: A decision assisted hybrid action space deep reinforcement learning approach,” *IEEE J. Sel. Areas Commun.*, vol. 42, no. 5, pp. 1029–1043, May 2024.
- [33] Z. Hu, F. Zeng, Z. Xiao, B. Fu, H. Jiang, H. Xiong, Y. Zhu, and M. Alazab, “Joint resources allocation and 3D trajectory optimization for UAV-enabled space-air-ground integrated networks,” *IEEE Trans. Veh. Technol.*, vol. 72, no. 11, pp. 14 214–14 229, Nov. 2023.
- [34] M. D. Nguyen, L. B. Le, and A. Girard, “Integrated computation offloading, UAV trajectory control, edge-cloud and radio resource allocation in SAGIN,” *IEEE Trans. on Cloud Comput.*, vol. 12, no. 1, pp. 100–115, Jan.-Mar. 2024.
- [35] J. Du, J. Wang, A. Sun, J. Qu, J. Zhang, C. Wu, and D. Niyato, “Joint optimization in blockchain and MEC enabled space-air-ground integrated networks,” *IEEE Internet Things J.*, to appear, 2024.
- [36] Y. Zeng, S. Chen, Y. Cui, J. Yang, and Y. Fu, “Joint resource allocation and trajectory optimization in UAV-enabled wirelessly powered MEC for large area,” *IEEE Internet Things J.*, vol. 10, no. 17, pp. 15 705–15 722, Sep. 2023.
- [37] M. D. Nguyen, L. B. Le, and A. Girard, “Joint computation offloading, UAV trajectory, user scheduling, and resource allocation in SAGIN,” in *Proc. IEEE Glob. Commun. Conf., GLOBECOM*, Virtual, Brazil, Dec. 2022, pp. 5099–5104.
- [38] Y. Zeng and R. Zhang, “Energy-efficient UAV communication with trajectory optimization,” *IEEE Trans. Wireless Commun.*, vol. 16, no. 6, pp. 3747–3760, Jun. 2017.
- [39] N. Zhang, H. Liang, N. Cheng, Y. Tang, J. W. Mark, and X. S. Shen, “Dynamic spectrum access in multi-channel cognitive radio networks,” *IEEE J. Sel. Areas Commun.*, vol. 32, no. 11, pp. 2053–2064, Nov. 2014.
- [40] C. Zhou, W. Wu, H. He, P. Yang, F. Lyu, N. Cheng, and X. Shen, “Deep reinforcement learning for delay-oriented IoT task scheduling in SAGIN,” *IEEE Trans. Wireless Commun.*, vol. 20, no. 2, pp. 911–925, Feb. 2021.
- [41] X. Zhang, W. Liu, H. Xing, Z. Jin, W. Zang, S. Wang, Y. Shen, and L. Xue, “Learning to hybrid offload in space-air-ground integrated mobile edge computing for IoT networks,” in *Proc. IEEE Int. Conf. CYBER Technol. Autom., Control, Intell. Syst., CYBER*, Qinhuangdao, China, Jul. 2023, pp. 836–841.
- [42] K. Shen and W. Yu, “Fractional programming for communication systems—Part I: Power control and beamforming,” *IEEE Trans. Signal Process.*, vol. 66, no. 10, pp. 2616–2630, May 2018.
- [43] O. Muñoz, A. Pascual-Iserte, and J. Vidal, “Joint allocation of radio and computational resources in wireless application offloading,” in *Proc. Future Netw. Mob. Summit*, Lisbon, Portugal, Jul. 2013, pp. 1–10.
- [44] Z.-q. Luo, W.-k. Ma, A. M.-c. So, Y. Ye, and S. Zhang, “Semidefinite relaxation of quadratic optimization problems,” *IEEE Signal Process. Mag.*, vol. 27, no. 3, pp. 20–34, May 2010.
- [45] W. Luo, Y. Shen, B. Yang, S. Wang, and X. Guan, “Joint 3-D trajectory and resource optimization in multi-UAV-enabled IoT networks with wireless power transfer,” *IEEE Internet Things J.*, vol. 8, no. 10, pp. 7833–7848, May 2021.
- [46] B. Chen, N. Li, Y. Li, X. Tao, and G. Sun, “Energy efficient hybrid offloading in space-air-ground integrated networks,” in *Proc. IEEE Wireless Commun. Netw. Conf., WCNC*, Austin, TX, United states, Apr. 2022, pp. 1319–1324.